Second-Harmonic Light Scattering by Domains In Ferroelectric Triglycine Sulfate†

G. Dolino, J. Lajzerowicz, and M. Vallade
Laboratoire de Spectrométrie Physique, Associé au Centre National de la Recherche Scientifique, Cedex 53-38-Grenoble, France
(Received 12 March 1970)

Second-harmonic generation and scattering has been studied in ferroelectric triglycine sulfate with a ruby laser. Theoretical considerations show that when the laser beam is incident in the optic plane, five scattered lines must exist with intensity depending upon the domain structure. Experimental data for angular positions of scattered lines are in good agreement with calculated values. The effect of laser polarization is also reported. Studies were made for multidomain and nearly single-domain crystals obtained by applying a dc electric field. An increase in the scattered intensity is observed when the domain pattern satisfies a Bragg condition.

I. INTRODUCTION

Many experiments of second-harmonic generation (SHG) have been performed with laser beams and the experimental results are well described by the theory of nonlinear interaction between plane waves.[1] The problem of the angular dependance of SHG is also well understood; Kleinman *et al.*[2] have given detailed solutions for SHG by focused laser beams. But far less attention has been paid to the phenomena of second-harmonic scattering (SHS); elastic as well as inelastic SHS were first reported in water.[3] Freund[4] observed nonlinear diffraction by plane-parallel domains in NH_4Cl in a direction satisfying a Bragg condition.

In this paper, we present results on SHS in triglycine sulfate (TGS) by ferroelectric domains. The domain structure of TGS, which is less simple than in NH_4Cl, leads to a more complicated pattern of scattered light, SHG in TGS has been previously studied by Smith,[5] and by Suvorov and Sonin,[6] who observed the influence of domains on SHG in the laser direction but did not investigate scattering. We have previously noted a broadening of the beam of SH around one direction and studied the effect on it of a dc electric field.[7]

Here a more complete description of the phenomena of SHS is given; we focused our attention on the optical aspects of the question rather than on the detailed behavior of the domains themselves.

In Sec. II, the theory of SHS by an inhomogeneous medium is discussed in terms of the Fourier transform. In Sec. III, this theory is applied to the TGS case and the existence of several scattered rays is shown. In Sec. IV, the experimental results are given when the laser beam is incident in the optic plane; the influence of thermal treatments and electric field on the scattering is also discussed for another geometry. Correlations between domains lead to an increase in the scattered intensity when a Bragg condition is satisfied.

II. THEORETICAL GENERAL FORMULATION

In this section, we solve, for a simple case, the problem of SHG by an inhomogeneous medium. For the sake of simplicity, we consider a nonlinear isotropic plane-parallel slab of refractive index $n_2(2\omega)$ immersed in a linear liquid of the same index. The linear optical properties are thus homogeneous in the whole space, the nonlinear source term $\vec{P}^{nls}(\vec{r})$ being the only inhomogeneous quantity. The electric field of the SH $\vec{E}_{2\omega}(\vec{r})$ is a solution of the Maxwell wave equation,[1]

$$\nabla\times\nabla\times\vec{E}_{2\omega}(\vec{r}) - (2\omega n_2/c)^2\vec{E}_{2\omega}(\vec{r}) = 4\pi(2\omega/c)^2\vec{P}^{nls}(\vec{r}) \tag{1}$$

with

$$\vec{P}^{nls}(\vec{r}) = \underline{\chi}(\vec{r}) : \vec{E}_\omega \vec{E}_\omega \exp(2i\vec{k}_1\cdot\vec{r}) \quad \text{inside the slab} \tag{2}$$

$$= 0 \text{ elsewhere.}$$

$\vec{E}_\omega$ is the electric field of the fundamental laser beam of wave vector $\vec{k}_1$. In ferroelectric crystals with centrosymmetric high-temperature phase, the nonlinear tensor $\underline{\chi}(\vec{r})$ is proportional to the static polarization $P^0(\vec{r})$[6, 8]:

$$\underline{\chi}(\vec{r}) = \underline{\chi}^0 P^0(\vec{r}) \ , \tag{3}$$

where $P^0(\vec{r})$ can take different values in a multidomain crystal. In the following, the z axis is taken normal to the slab of thickness l, which is then represented by a form function

$$B(\vec{r}) = Y(z+\tfrac{1}{2}l) - Y(z-\tfrac{1}{2}l) \ ,$$

where

$$Y(z)=0 \text{ if } z<0, \quad Y(z)=1 \text{ if } z>0 . \tag{4}$$

Equation (2) can thus be rewritten as

$$\vec{P}^{\text{nls}}(\vec{r})=\underline{\chi}^0 P^0(\vec{r}) B(\vec{r}): \vec{E}_\omega \vec{E}_\omega \exp(2i\vec{k}_1\cdot\vec{r}) . \tag{2'}$$

Neglecting the effect of the finite dimensions of the slab on the internal domain structure, we can take the Fourier transform of (2'),

$$\vec{P}^{\text{nls}}(\vec{k})=\int [d^3r/(2\pi)^3]\,\vec{P}^{\text{nls}}(\vec{r})\,e^{-i\vec{k}\cdot\vec{r}}$$

$$=\underline{\chi}^0: \vec{E}_\omega \vec{E}_\omega \int d^3q\, P^0(\vec{q})\, B(\vec{k}-(2\vec{k}_1+\vec{q})) , \tag{5}$$

where

$$B(\vec{k})=\delta(k_x)\,\delta(k_y)\,\sin(\tfrac{1}{2}k_z)(\pi k_z)^{-1} . \tag{6}$$

The Fourier transform of $\vec{E}_{2\omega}(\vec{r})$ is given by

$$\vec{E}_{2\omega}(\vec{k})=\vec{C}\int d^3q\, P^0(\vec{q})\, B[D^-(\vec{k})][|\vec{k}|^2-(2\omega n_2/c)^2]^{-1} , \tag{7}$$

with

$$\vec{C}=4\pi(2\omega/c)^2\chi^0: \vec{E}_\omega \vec{E}_\omega , \tag{8}$$

$$D^\pm(\vec{k})=\vec{k}\pm(2\vec{k}_1+\vec{q}) . \tag{9}$$

We can now calculate $\vec{E}_{2\omega}(\vec{r})$ by taking the inverse Fourier transform of Eq. (7).

Defining a wave vector $\vec{k}_2$ by

$$\begin{aligned} k_{2x}&=2k_{1x}+q_x , \\ k_{2y}&=2k_{1y}+q_y , \\ k_{2z}&=[(2\omega n_2/c)^2-k_{2x}^2-k_{2y}^2]^{1/2} , \end{aligned} \tag{10}$$

we obtain

$$\vec{E}_{2\omega}(\vec{r})=\vec{C}\int d^3q\, P^0(\vec{q})\exp[i(k_{2x}x+k_{2y}y)]$$

$$\times\int dk_z \frac{\exp(ik_z z)\sin[\frac{1}{2}D^-(k_z)l]}{(k_z^2-k_{2z}^2)D^-(k_z)} . \tag{11}$$

The last integral is easily calculated by expanding the integrand into a sum of three rational fractions and remembering that

$$\lim_{\epsilon\to 0^+}\int dk\, \frac{\exp\{i[k\pm(k_2+i\epsilon)]z\}}{2i\pi[k\pm(k_2+i\epsilon)]}=\mp Y(\mp z) . \tag{12}$$

Finally,

$$\begin{aligned} \vec{E}_{2\omega}(\vec{r})=\vec{C}\int d^3q\, P^0(\vec{q})\exp[i(k_{2x}x+k_{2y}y)]\Bigg(&\frac{Y(z+\tfrac{1}{2}l)-Y(z-\tfrac{1}{2}l)}{-D^-(k_{2z})D^+(k_{2z})}\exp[i(2k_{1z}+q_z)z] \\ &+\frac{[Y(z+\tfrac{1}{2}l)\exp(\tfrac{1}{2}iD^-(k_{2z})l)-Y(z-\tfrac{1}{2}l)\exp(-\tfrac{1}{2}iD^-(k_{2z})l)]}{2k_{2z}D^-(k_{2z})}\exp(ik_{2z}z) \\ &-\frac{[Y(-z-\tfrac{1}{2}l)\exp(-\tfrac{1}{2}iD^+(k_{2z})l)-Y(-z+\tfrac{1}{2}l)\exp(+\tfrac{1}{2}iD^+(k_{2z})l)]}{2k_{2z}D^+(k_{2z})}\exp(-ik_{2z}z)\Bigg) . \end{aligned} \tag{13}$$

Equation (13) gives the field in the whole space, both for backward and forward travelling waves. In our experiments we are essentially interested in the field radiated with a given wave vector k_2 in the half-space $z>\frac{1}{2}l$:

$$\begin{aligned} \vec{E}_{2\omega,\vec{k}_2}(\vec{r})&=(\tfrac{1}{2}\vec{C}/k_{2z})\exp(i\vec{k}_2\cdot\vec{r})\int d^3q\, P^0(\vec{q})\delta(D^-(k_{2x}))\,\delta(D^-(k_{2y}))\,\{2i\sin[\tfrac{1}{2}D^-(k_{2z})l]\}/D^-(k_{2z}) \\ &=(i\pi\vec{C}/k_{2z})\exp(i\vec{k}_2\cdot\vec{r})\int d^3q\, P^0(\vec{q})\, B(\Delta\vec{k}-\vec{q}) \end{aligned} \tag{14}$$

with

$$\Delta\vec{k}=\vec{k}_2-2\vec{k}_1 .$$

So we recognize in Eq. (14) the convolution product of the Fourier component $P^0(\vec{q})$ of the polarization by the Fourier component $B(\Delta\vec{k})$ of the form factor. [We note that the SHG by an homogeneous slab appears as a particular case of Eq. (14) where $P^0(\vec{q})=P^0\delta(\vec{q})$.] If the thickness $l\to\infty$, $B(\Delta\vec{k}-\vec{q})\to\delta(\Delta\vec{k}-\vec{q})$ and

$$\vec{E}_{2\omega,\vec{k}_2}(\vec{r})\to(i\pi\vec{C}/k_{2z})\;P^0(\Delta\vec{k})\exp(i\vec{k}_2\cdot\vec{r}) . \tag{15}$$

In this approximation, the intensity scattered in a given direction $\vec{k}_2$ appears to be proportional to $|P^0(\Delta\vec{k})|^2$, i.e., the $\Delta\vec{k}$ component of the Fourier transform of the correlation function of the static polarization. Such a result can also be obtained using spherical waves and a Green's-function

formalism as has been done for a focused beam in homogeneous media.[2]

III. SECOND HARMONIC IN TGS

TGS is a ferroelectric crystal with a Curie temperature of 49 °C; its point group is $2/m$ for the paraelectric phase and 2 for the polar phase[9]; so it is biaxial in both the phases and the acute bisector of the optic axes lies along the monoclinic axis, i.e., the ferroelectric axis. As is conventional, we call this direction $0Y$. But $0Z$, which is usually taken parallel to the c axis of the unit cell and is nearly perpendicular to the optic plane, is here taken strictly perpendicular to this plane.[5] In the following the small dispersion of the optic plane will be neglected. TGS crystals show antiparallel domains, the physical properties of which are related to each other by the center of symmetry which changes the polarization into its opposite. (This is the symmetry operation which is lost at the transition.) In particular, the index ellipsoid which has an axis parallel to $0Y$ is invariant in this symmetry and therefore the linear optical properties of the two kinds of domains are identical. So, the domain structure cannot be studied by ordinary optical means.[10] On the other hand, the nonlinear optical susceptibility which is proportional to the spontaneous polarization is reversed on going from one domain to the next one. The components of the nonlinear polarization are

$$\begin{aligned} P_x &= \chi_{14} E_y E_z + \chi_{16} E_x E_y \,, \\ P_y &= \chi_{21} E_x E_x + \chi_{22} E_y E_y + \chi_{23} E_z E_z + \chi_{25} E_z E_x \,, \\ P_z &= \chi_{34} E_y E_z + \chi_{36} E_x E_y \,, \end{aligned} \tag{16}$$

where each element of the nonlinear tensor $\underline{\chi}$ is proportional to the spontaneous polarization.[6]

If we consider a plane-parallel slab of TGS, the optic plane of which is taken as the incidence plane, the SHG by a laser beam of external wave vector $\vec{k}_1$ is described in Fig. 1. There are three nonlinear source waves which propagate with wave vectors:

$$\vec{K}_{oo} = 2\vec{k}_{1o} \,, \tag{17a}$$

$$\vec{K}_{ee} = 2\vec{k}_{1e} \,, \tag{17b}$$

$$\vec{K}_{oe} = \vec{k}_{1o} + \vec{k}_{1e} \,, \tag{17c}$$

where subscripts o and e refer, respectively, to ordinary and extraordinary waves. For a single-domain crystal, SH waves propagate in the slab with wave vectors $\vec{k}_{2o}$ and $\vec{k}_{2e}$. These two rays, which have the same tangential component along the surface, give only one emerging beam with wave vector $\vec{k}_{2N}$ (in a direction different from $\vec{k}_1$ if the external medium is dispersive). In the optic plane, there are two directions of phase matching

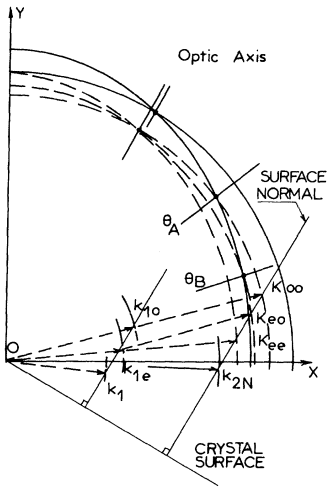

FIG. 1. Laser-beam propagation in the optic plane of TGS. Wave vectors and refractive-index curves of the fundamental waves are shown by dotted lines. Those of SH are shown by full lines.

noted θ_A (where $2\vec{k}_{1o} = \vec{k}_{2e}$) and θ_B (where $\vec{k}_{1o} + \vec{k}_{1e} = \vec{k}_{2e}$).

For a multidomain crystal, other harmonic waves propagate, the wave vectors of which obey the relation $\vec{k}_2 = \vec{K} + \vec{q}$, with an intensity proportional to $|P^0(\vec{q})|^2$, where $P^0(\vec{q})$ is the $\vec{q}$ component of the Fourier transform of the static polarization. In TGS the domains are long cylinders parallel to $0Y$ with lenticular cross sections ranging from a few tens to some hundreds of microns. So we expect $P^0(\vec{q})$ to be most important for $\vec{q}$ lying in the $X0Z$ plane. Figure 2 shows that, following this assumption, there are inside the crystal six directions of propagation for scattered light in the optic plane given by

$$\begin{aligned} \vec{k}_{2eA} &= \vec{K}_{oo} + \vec{q}_A, & \vec{k}_{2oD} &= \vec{K}_{oo} + \vec{q}_D \,, \\ \vec{k}_{2eB} &= \vec{K}_{eo} + \vec{q}_B, & \vec{k}_{2oE} &= \vec{K}_{eo} + \vec{q}_E \,, \\ \vec{k}_{2eC} &= \vec{K}_{ee} + \vec{q}_C, & \vec{k}_{2oF} &= \vec{K}_{ee} + \vec{q}_F \,. \end{aligned} \tag{18}$$

Near the laser direction one can predict six lines of scattered harmonic light perpendicular to $0Y$ (in addition to the usual SH peak), with intensities determined by the corresponding $P^0(\vec{q})$ the magnitude of which depends on the ratio of the domain width to the coherence length $l_c = \pi/|\vec{q}|$ and by the values of the various coefficients of the nonlinear susceptibility tensor. So the scattering corresponding to $\vec{q}_D$ is forbidden in the optic plane because it would be produced by the tensor element χ_{33} which is zero. Conversely, knowing the susceptibility tensor, and measuring the scattered

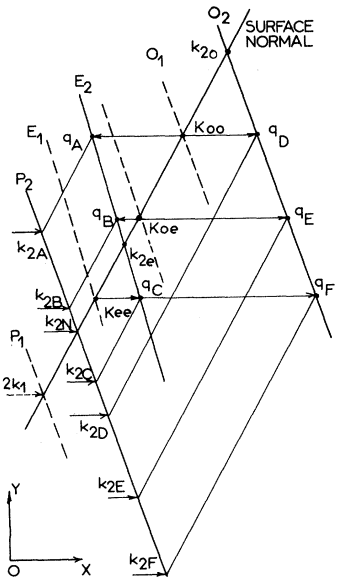

FIG. 2. Extremities of wave vectors in the optic plane of TGS for a multidomain crystal. Dotted lines denote fundamental, solid lines SH waves. $P_{1,2}$: refractive indices curve of external medium; $E_{1,2}$: refractive indices curve of extraordinary wave; $O_{1,2}$: refractive indices curve of ordinary wave. (Subscripts 1 and 2 refer, respectively, to fundamental and harmonic waves.)

intensities one may get an idea of the correlation function of the polarization.

IV. EXPERIMENTAL RESULTS

In this section, the experimental verification of the SHS laws in TGS is presented. The experimental setup used is shown in Fig. 3. The beam of a Q-switched ruby laser (30-MW peak power, 3×10^{-3}-rad beam divergence) is focused by a 1000-mm focal-length lens on a TGS slab. SHG

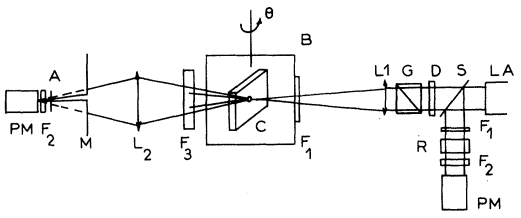

FIG. 3. Experimental setup. LA: Q-switched ruby laser; S: 15% beam splitter; F_1: red filter; F_2: interference uv filter; R: ADP reference crystal; PM: photomultiplier; D: attenuators; L_1: 1000-mm focal-length lens; B: temperature controlled paraffin oil bath; C: TGS crystal; θ: vertical axis of rotation; F_3: $CuSO_4$ cell; L_2: quartz collection lens; M: movable aperture in the focal plane of L_2; A: analyser.

is detected with a photomultiplier and compared to the SHG of a monitoring ADP crystal; the incident beam can be polarized by a Glan prism and be attenuated by filters. The sample is immersed in a temperature-controlled paraffin oil bath which matches approximately the refractive index of the crystal and so reduces spurious surface scattering. SH is collected by a 200-mm focal-length lens in the focal plane of which is mounted a small movable aperture to observe the angular dependence of harmonic light.

A. Experimental Evidence of SHS

The first crystal studied (sample I) was a 10 $\times10\times3$-mm plane-parallel slab cut nearly normal to an optic axis. A conoscopic observation method[11] was used to set the optic plane perpendicular to a vertical rotation axis and to direct the laser beam parallel to this plane.

The measured angles of optic axis and phase matching directions are summarized in Table I. The refractive indices of TGS and paraffin oil for fundamental and harmonic light are given in Table II. TGS indices are extrapolated from published values,[12,13] but for the harmonic region, extrapolation is not sufficiently accurate and it was necessary to fit them to give observed phase-matching angles. (These values are consistent with extrapolated ones.)

SH intensity distribution in the focal plane of the collection lens for an angle of incidence of $+26°$ is shown in Fig. 4. One notices a central circular peak with the same angular width as the laser beam corresponding to the usual SH beam. As expected, SH scattering is line-shaped perpendicularly to $0Y$ (vertical lines on Fig. 4). The two intense parallel lines are extraordinary scattered light; the third extraordinary ray is weaker for this incidence angle. The two ordinary scattered lines, still weaker, are easily observed by selecting the right polarization with an uv polaroid analyzer. When the incidence angle is changed, the angular positions of the lines are shifted: Theoretical and

TABLE I. Measured external incidence angle θ and corresponding calculated internal angle ψ for a crystal immersed in paraffin oil, with the incidence plane in the optic plane (sample I).

	θ	ψ
Optical axis V_1	−65°25′	−30°50′
$0Y$		0
Surface normal	0	+28°30′
Optical axis V_2	+ 2°30′	+30°50′
Phase matching A	+21°20′	+48°30′
Phase matching B	+37°50′	+63°50′

TABLE II. Refractive indices of TGS and paraffin oil for fundamental (ω) and second harmonic (2ω).

	TGS			Paraffin oil
	n_x	n_y	n_z	n_p
ω	1.580	1.482	1.553	1.468
2ω	1.6184	1.5072	1.5865	1.495

experimental results are represented in Fig. 5. Calculated values are deduced from the data of Tables I and II by using Snell laws. The dependence of the intensity of the lines on the polarization of the laser beam is shown in Table III. It agrees well with theoretical predictions. The variations of intensities with rotation of the crystal are a function of the detailed domain structure, but when approaching a phase-matching direction, one of the scattered lines and the central peak increase in intensity and merge together.

B. Effect of dc Field

The second sample is oriented in a different manner in order to apply an electric field: it is a 10×10×6-mm parallelepiped, the square faces of which are provided with silver-painted electrodes. The normals to the entrance face and to the electrodes lie in the optic plane, the former making an angle of 40° with $0Y$ in order to separate the different scattered lines. The rotation axis is perpendicular to the electrodes. The salient features of SHS are the same as for the previous geometry but one can now see the six scattered lines. To examine the influence of the domain structure it is convenient to observe the intensity integrated over all scattering directions for different thermal treatments and applied electric fields. Figure 6 shows the variations of this intensity as a function of incidence angle near a phase-matching direction. Curve I corresponds to temperature higher than the Curie point (60 °C): the presence of SH in the paraelectric phase was already noted by Suvorov and Sonin, [6] who attributed

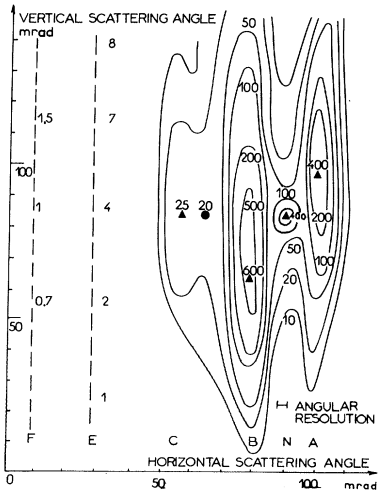

FIG. 4. Intensity contours of extraordinary SH light in the focal plane of the collection lens. The two ordinary lines are too weak to be drawn in detail. Their positions are indicated by the two dotted lines on the left. Numbers indicate SH intensity in arbitrary units (constant throughout this paper). Scattering angles are measured in air at room temperature (sample I).

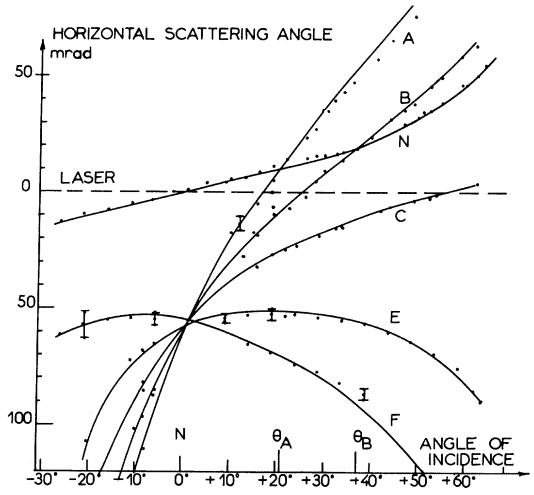

FIG. 5. Angular positions in air of the five scattered lines (A to F) and of the normal peak (N) of SH as a function of incidence angle (sample I). Solid line: calculated values. Dots: experimental points.

TABLE III. Dependence of SH intensity (arbitrary units) of the five scattered lines (A to F) as a function of polarization of the fundamental light, incident in the optic plane (sample I) (measured at various incidence angles θ indicated in the right-hand column). o: vertical polarization, only one ordinary laser beam; oe: polarization at $\frac{1}{4}\pi$ from the optic plane, ordinary, and extraordinary laser beams; e: horizontal polarization, only one extraordinary laser beam.

Scattered line	o	oe	e	θ
A	750	500	0	+25°
B	20	500	20	+25°
C	0	100	200	+60°
E	0	30	0	+25°
F	0	80	120	−16°

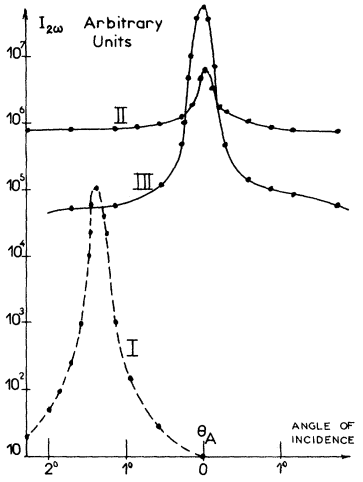

FIG. 6. Second-harmonic intensity $I_{2\omega}$ near phase matching A for sample II (plane of incidence different from the optic plane). Curve I at temperature $T = 60\,^{\circ}C$ (paraelectric phase). Curve II at room temperature after rapid cooling under a 400-V/cm ac electric field. Curve III at room temperature after slow cooling under a 5000-V/cm dc electric field.

it to residual domains. Considering the sharpness of curve I this seems unlikely, but it is very difficult to say whether SH has a quadrupolar or dipolar origin because the intensity in mismatching directions is too low to allow a study of the form of the susceptibility tensor. Curves II and III are drawn at room temperature; the former after a rapid cooling from the paraelectric phase (10 min to go from 60 to 25 °C) with a 400-V/cm ac electric field so as to have a multidomain structure; the latter after a slow cooling (5 h) with a 5-kV/cm dc field in order to get a single-domain sample. This was not completely successful since the foot of the peak is still broad.

Nevertheless the difference between curves II and III can be explained by considering that the crystal has many domains in the first case and is almost single domain with small residual domains in the second case. This fact has been verified by making an angular study of scattered light. In the first case the scattered lines are stronger than in the second by an order of magnitude, whereas the phase-matching central peak is very much weaker.

C. Bragg Diffraction

In Fig. 7 another interesting feature can be seen when observing the integrated intensity as a function of incidence angle near a phase-matching direction, at a temperature a few degrees below the Curie point, after a thermal shock. There are two maxima, symmetric about the phase-matching direction and a detailed study shows that they are due to a scattered peak corresponding to a $\vec{q}$ nearly perpendicular to the optic plane. This observation recalls that of Freund[4] in NH_4Cl and may be explained by a regular periodic domain structure with a period of about 10 μ nearly parallel to the optic plane.[14] As was already noted, this is closely analogous to a Bragg diffraction.

V. CONCLUSION

The experimental observations of SHS in TGS agree very well with theoretical predictions for angular separations and polarizations of the scattered lines. This phenomena can be used as a tool for studying properties of domains which cannot be seen by ordinary optical means. Its advantage over the etching method[9,14] is that it allows continuous observations as a function of temperature or applied electric field although a quantitative interpretation seems difficult. Systematic measurements, mainly in the vicintity of the Curie point, are currently under way.

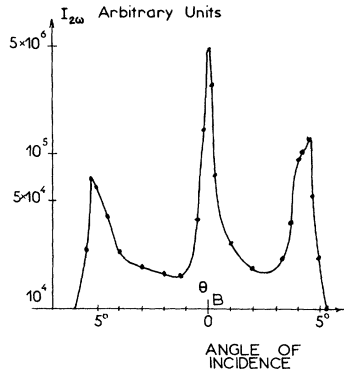

FIG. 7. Second-harmonic intensity $I_{2\omega}$ versus incidence angle near phase matching B for sample I showing Bragg diffraction by an almost regular domain array ($T = 45\,^{\circ}C$).

†Work partially supported by Délégation Générale à la Recherche Scientifique et Technique.

[1]N. Bloembergen, *Nonlinear Optics* (Benjamin, New York, 1965).

[2]D. A. Kleinman, A. Ashkin, and G. D. Boyd, Phys. Rev. 145, 338 (1966).

[3]R. W. Terhune, P. D. Maker, and C. M. Savage, Phys. Rev. Letters 14, 681 (1965).

[4]I. Freund, Phys. Rev. Letters 21, 1404 (1968).

[5]A. W. Smith, Appl. Opt. 3, 147 (1964).

[6]V. S. Suvorov and A. S. Sonin, Zh. Eksperim. i Teor. Fiz. 54, 1044 (1968) [Soviet Phys. JETP 27, 557 (1968)], and references therein.
[7]G. Dolino, J. Lajzerowicz, and M. Vallade, Solid State Commun. 7, 1005 (1969).
[8]R. C. Miller, Phys. Rev. 134, A1313 (1964).
[9]F. Jona and G. Shirane, *Ferrolectric Crystals* (Macmillan, New York, 1962).
[10]Nevertheless, one optical observation has been reported: S. M. Shapiro, R. W. Gammon, and H. Z. Cummins, Appl. Phys. Letters 10, 113 (1967).
[11]Bruhat-Kastler, *Optique* (Masson, Paris, 1965).
[12]L. G. Lomova, A. S. Sonin, and T. A. Regusl'skaya, Kristallografiya 13, 90 (1968) [Soviet Phys. Crist. 13, 68 (1968)].
[13]H. Iwasaki and H. Toyoda, Japan J. Appl. Phys. 7, 787 (1968).
[14]F. Moravets and V. P. Konstantinova, Kristallografiya 13, 284 (1968) [Soviet Phys. Crist. 13, 221 (1968)], and references therein.

PHYSICAL REVIEW B VOLUME 2, NUMBER 6 15 SEPTEMBER 1970

Theory of One- and Two-Phonon Reorientation Rates of Paraelectric Defects in Ionic Crystals*

B. G. Dick and D. Strauch†
Department of Physics, University of Utah, Salt Lake City, Utah 84112
(Received 9 February 1970)

A theory of one- and two-phonon-assisted reorientation rates of substitutional OH^- ions in alkali-halide crystals has been developed. We treat the case of reorientation of dipoles preferring ⟨100⟩ directions with a large static applied electric field in a ⟨100⟩ direction. We use unperturbed breathing shell-model phonons and a dipole-lattice Hamiltonian which includes both one- and two-phonon operators and which is not limited in its validity to the long-wave limit. The theory is applied primarily to OH^- in RbBr with good qualitative agreement with experiment. In particular, we find an approximate T^4 dependence of relaxation rate due to two-phonon Raman-type processes in the 5–10 °K temperature range, in agreement with experiment. Our theory also agrees with experiment in its prediction that two-phonon reorientation processes will begin to dominate one-phonon processes above a temperature of about 4 °K. In the temperature range studied, those two-phonon reorientation rates produced by the one-phonon operators in the dipole-lattice interaction Hamiltonian acting twice exceed by several orders of magnitude the two-phonon reorientation rates produced by the interaction Hamiltonian two-phonon operators acting once. Similar results are found for OH^- in KBr and KCl.

I. INTRODUCTION

There have been several recent studies of the theory of reorientation processes for paraelectric[1,2] and paraelastic[3–6] defects in ionic crystals. These studies all have the feature of using a dipole-lattice interaction Hamiltonian which is valid only for long-wave phonons; also, Debye or other approximate dispersion relations for the phonons have been used. While these approximations are adequate for treating one-phonon-assisted tunneling reorientation processes in attainable electric fields, they are not adequate for two-phonon processes which become important above about 5 °K. In this paper we shall be concerned mainly with an effort to use more realistic models for the phonons and the phonon-defect interaction than have been used heretofore to investigate the one- and two-phonon-assisted tunneling rates of OH^- defects in alkali-halide crystals with a large electric field applied in a ⟨100⟩ direction. We have developed a dipole-lattice interaction Hamiltonian which includes both one- and two-phonon operators and which is not restricted to the long-wave limit, as previously used forms of this interaction Hamiltonian have been. Our treatment gives a very good qualitative account of the temperature and electric field dependence of observed relaxation rates for OH^- in RbBr from 1.35 to 12.5 °K, as well as for OH^- in other alkali-halide hosts for which the relaxation rates are not known over such a wide temperature range. From this study we can acquire new information about the phonon-defect interaction which one hopes may eventually be useful in unraveling some of the puzzles concerning the infrared absorption of these systems.[7] This information also should provide a starting point for a study of the perturbation of the phonons due to